Measuring the microelastic properties of biological material

N. J. Tao,* S. M. Lindsay,* and S. Lees‡
*Department of Physics, Arizona State University, Tempe, Arizona 85287; and
‡Bioengineering Department, Forsyth Dental Center, Boston, Massachusetts 02115

ABSTRACT We have used the atomic force microscope (AFM) to measure the local rigidity modulus at points on the surface of a section of hydrated cow tibia. These data are obtained either from contrast changes that occur as the contact force is altered, or from force versus distance curves obtained at fixed points. These two methods yield the same values for rigidity modulus (at a given point). At low resolution, the elastic morphology and topography mirror the features seen in optical and electron micrographs. At high resolution we see dramatic variations in elastic properties across distances as small as 50 nm.

INTRODUCTION

The atomic force microscope (1) has been used to image surfaces with atomic resolution (2), to measure tip-surface interactions (3, 4), atomic-scale friction (5, 6), and magnetic (7) and electric (8) interactions. It has been used as a "nanoindenter" to measure the elastic properties of various surfaces (9, 10) and (by an ac modulation technique) as a method for mapping the relative stiffness of the surface of a carbon fiber composite (11). Here, we described how we have used the microscope to measure the small scale (~50 nm) variations in the elastic properties of a biological composite material (bone) in which the details of the matrix play a crucial role in its macroscopic elastic properties. We show how both force versus distance curves and images taken at various contact forces can be used to obtain quantitative data.

Bones have rather complicated but well organized structures. The relationship between their structures and elastic properties is still not well understood. Ultrasonic (12, 13), spectroscopic (14–17), and mechanical (18) methods have been used to probe their elastic properties on macroscopic length scales. Detailed structural information has been obtained from optical microscopy, x-ray diffraction, and electron microscopy (19). The data we report here correlate the elastic and topographic features on a hitherto inaccessible scale.

MATERIALS AND METHODS

In this study, we used a piece of cow tibia cut perpendicular to the axial direction. The bone was polished with diamond grit down to 0.3 μm particle size and washed in deionized water between successive grits. It was wetted with 0.15 M saline solution containing 0.04% sodium azide.

The AFM measurements were performed under water or saline to preserve hydration because the elastic properties of these materials depend upon their water content (12–17). Images were obtained in the constant-force mode using a Nanoscope II AFM from Digital Instruments Inc. (Santa Barbara, CA). Cantilevers with tips were also supplied by Digital Instruments. Cantilevers were calibrated by measuring their deflection when pushed with calibrated glass fibers. The fibers were calibrated by measuring their deflection when loaded with small weights.

The AFM works by detecting interactions between a tip on a cantilever and the surface of a sample. For samples that are soft (relative to the cantilever spring constant) the interaction produces a significant deformation of the sample. In a homogeneous elastic material, this deformation can be used to extract the shear modulus of the substrate if the tip geometry is known. A complex composite like bone is inhomogeneous down to the ultrastructural level where collagen and mineral interact (length scales of ~10 nm). However, our data show that the elastic morphology correlates with the topography very well. Furthermore, resolution of the boundaries between regions of different rigidity modulus is comparable to the topographical resolution of the AFM. A continuum elasticity theory is therefore an appropriate starting point until an appropriate microscopic model can be established.

The AFM tips we used in these experiments are pyramidal corners of microfabricated Si_3N_4. In our calculations, we have approximated the pyramids as cones of semivertical angle 72° and used Sneddon's (20) results for the force dependence of the penetration of a punch to calculate the deformation profile. This profile depends only on the geometry of the cone. Thus, while the result shown in the inset has been (arbitrarily) calculated for a penetration depth of 50 nm, the overall shape will be the same at all depths. In consequence, the lateral extent of contact is always about equal to the penetration depth for a cone of this angle. The penetration depth was a maximum of ~10 nm for the force distance measurements and varied between 3 and 50 nm for the images (depending upon the force used). Therefore, we expect that the resolution will be equal to or better than 50 nm, an expectation borne out by the finest structures observed in our images. This discussion suggests that a continuum analysis is valid if the scale of the (ultrastructural) inhomogeneities is less than the deformation depth.

If a force, F, is applied by a conical tip of semivertical angle α to a surface of shear rigidity, G, and Poisson's constant, σ, the resulting deformation, D, is given by (20):

$$D^2 = \frac{\pi(1-\sigma)F}{4G\cot(\alpha)}. \quad (1)$$

The contact force is given by the measured cantilever deflection, δz, multiplied by the cantilever spring constant, k. The deformation, D, is $z - \delta z$, where z is the distance between the sample and the undeflected cantilever (this analysis assumes that the sample thickness [mm] is greater than the [nm] penetration). This is the experimental quantity obtained from the distance that the z transducer moves after contact. Inserting these variables into Eq. 1 and solving for δz yields:

$$\delta z = z + \frac{k}{2A}\left[1 - \sqrt{1 + \frac{4Az}{k}}\right], \quad (2)$$

where $A = 4G\cot(\alpha)/\pi(1-\sigma)$ and we have taken the negative root because the positive root corresponds to a finite deformation at $z = 0$, an unphysical result. Thus, by fitting experimental curves for δz vs. z with Eq. 2, the quantity $G/(1-\sigma)$ may be obtained. Note that for a very stiff surface ($G \gg k$) $\delta z = z$ (the slope of the plot is unity). The amount of

0006-3495/92/10/1165/05 $2.00

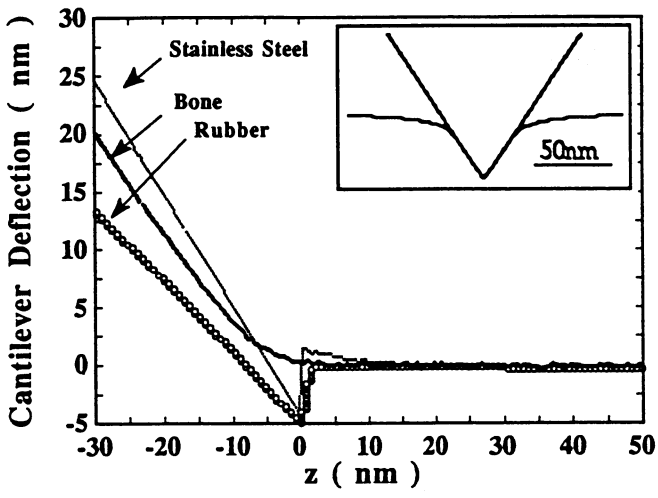

FIGURE 1 Cantilever deflection vs. z scan. Curves are for the tip over stainless steel, a soft region of cow tibea in an osteonal lamellum and a piece of rubber. The inset is the calculated deformation under a conical punch (with a semivertical angle of 72°) according to Sneddon's theory (20). The profile is shown for a deformation depth of 50 nm and a cone angle of 72°.

departure from $z = \delta z$ is the deformation D. Data taken at least 10 nm from the initial contact point do fit the D^2 dependence on force predicted by Eq. 1. Closer to contact, the interaction is often complicated by the effects of attractive forces not considered here.

The point of contact (in the absence of tip deformation) must be found in order for the correct zero of the z scale to be established, and this cannot be measured precisely because of the complexity of the interaction as tip approaches the surface; under solution, the uncertainty is quite small (a few nanometers) compared with the distance changes over which data are taken and the effect of this uncertainty on the slope used for determining G is negligible.

RESULTS AND DISCUSSION

We show measured plots of δz vs. z in Fig. 1. Data are for a clean stainless steel disk, a soft part of the bone and a piece of rubber (cut from an eraser). The slope of the plot for steel is unity so G cannot be determined ($G \gg k$). For the rubber the slope is much less than one: it is 0.57 at $z = 20$ nm, which, with $k = 0.58$ N/m (as determined by our calibration), yields $G = 1.3 \times 10^7$ N/m^2 with $\sigma = 0.5$ for rubber. We also determined G for the same piece of rubber using macroscopic indentation with a ball bearing, obtaining 1.1×10^7 N/m^2 (using the appropriate form of Sneddon's results [20]). The good agreement between the macroscopic and microscopic measurements indicates that the assumption of a conical tip geometry for the AFM is reasonable. Microscopic rigidity moduli for the bone sample were measured from the δz vs. z curves by placing the tip over a specific structure as described below. The results were also checked by imaging the sample under different forces.

Fig. 2 *a* is a typical low magnification AFM image obtained under a constant repulsive force of 2.9 nN. It shows the familiar Haversian system seen in optical microscopy (21) (we have deliberately selected an unusually small system so as to fit it into the scan range of the AFM). The Haversian canal, osteonal lamellae, and interstitial lamellae (21) are labeled as HC, HL, and IL. For comparison, an optical micrograph of our sample is shown in Fig. 3. The Haversian canal shown in Fig. 3 is about twice the size of the Haversian canal shown in the AFM images (Fig. 2). Fig. 2 *b* is an image of the same area shown in Fig. 2 *a* but taken under a force of 205 nN. Though the image is similar to that obtained under small force, the relative height of the osteonal lamellae to the interstitial lamellae is clearly increased (by ~45 nm). This means that the osteonal lamellae are deformed less than the interstitial lamellae and must, therefore, be stiffer in this surface region. Using Eq. 1, we estimated G of the interstitial lamellae to be in the range 0.06 to 0.08 GPa (for σ in the range 0.4 to 0.2 [22]). The image obtained when the force was changed back to 2.9 nN is

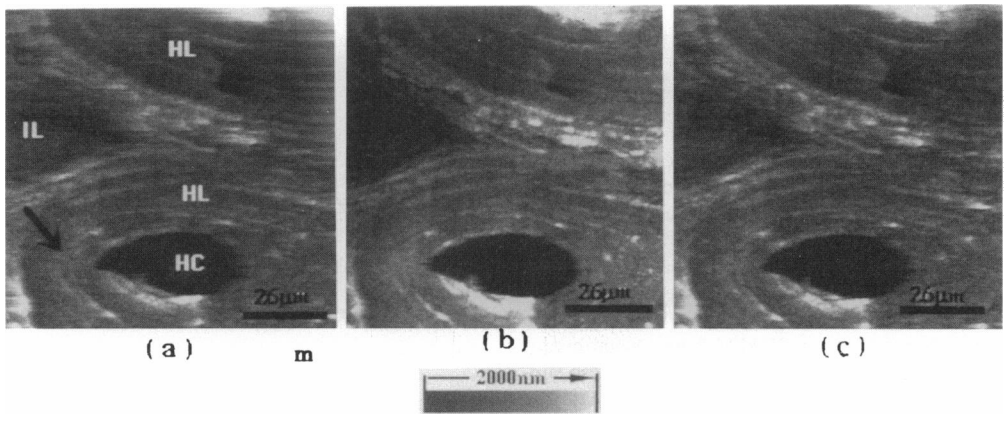

FIGURE 2 Large scale (110,000 × 110,000 nm) AFM images of cow tibia (view from the axial direction). A small Haversian system was chosen to show as much detail as possible within the limited scan range of the AFM. Images are obtained under water and contact forces of 2.9 nN (*a*), 205 nN (*b*), and 2.9 nN (*c*). The osteonal lamellae, Harversian canal, and interstitial lamellae are indicated by HL, HC, and IL. The vertical distance between the interstitial lamellae and the osteonal lamellae is clearly increased under 205 nN.

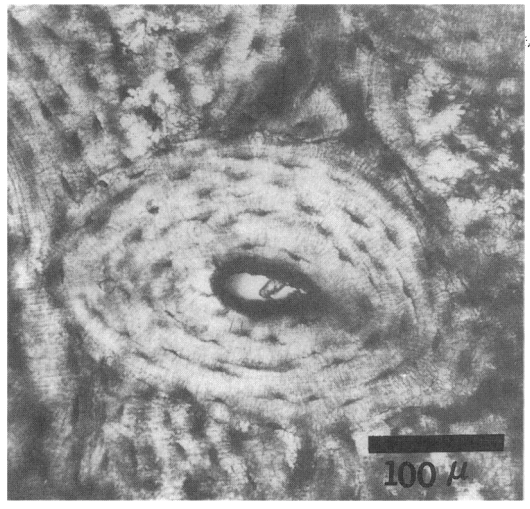

FIGURE 3 Optical micrograph of the surface of the sample used in this study.

shown in Fig. 2 *c*. The original contrast is nearly completely recovered, indicating that the deformation under 205 nN load is still elastic. We also obtained the rigidity moduli of the osteonal and interstitial lamellae by measuring more than 30 δz vs. z curves over each region. We obtained rigidity moduli in the range 0.7 to 0.9 GPa for the osteonal lamellae. These values are similar to the rigidity modulus of pure collagen fibers (~1 GPa) measured by macroscopic methods (14). Similar measurements give 0.1 to 0.13 GPa for the interstitial lamellae, which is consistent with the estimate from the images taken under different forces. We have conducted the same measurements on many osteonal and interstitial lamellae and found that the osteonal lamellae appear to be more rigid than the interstitial lamellae in this surface region (with a few exceptions).

Higher magnification images of an osteonal lamellum under 2.5, 209, and 2.5 nN are shown in Fig. 4, *a, b,* and *c,* respectively. There are two bright stripes at the centers of these images. The contrast of the stripes decreases as the force is increased to 209 nN, but it is fully recovered as the force is changed back to 2.5 nN. These features are thus more deformable than the background and, again, the deformation is elastic under a force of 209 nN. The average G of the bright stripes was estimated to be in the range 0.2 to 0.25 GPa from the change of the relative deformation (~22 nm).

Even higher magnification images taken under 2.5, 205, and 2.5 nN forces are shown in Fig. 5, *a–c.* Fig. 5 *a* shows "blobs" of various size from 50 to 500 nm. These features are not revealed by conventional microscopy and their structure is unknown. Under 205 nN force, the boundaries of the "blobs" blurred out. This suggests that the regions between the "blobs" are more rigid than the "blobs". We have measured δz vs. z curves on "blobs" and on regions between the "blobs", finding that the rigidity of the "blobs" lies in the range 0.7 to 0.9 GPa, whereas the rigidity between the "blobs" is estimated to be greater than 10 GPa (too rigid to be measured). These very large differences suggest a very different composition between the two regions (inter- and intra-"blob"). On changing the force back to 2.5 nN the image is only partially recovered. Thus, on this length scale, deformation is not elastic at 205 nN. The damage must be quite local, however, for neither the elastic properties or topography are affected at the larger length scales.

We have also measured the macroscopic rigidity modulus of the sample using indentation with a ball bearing.

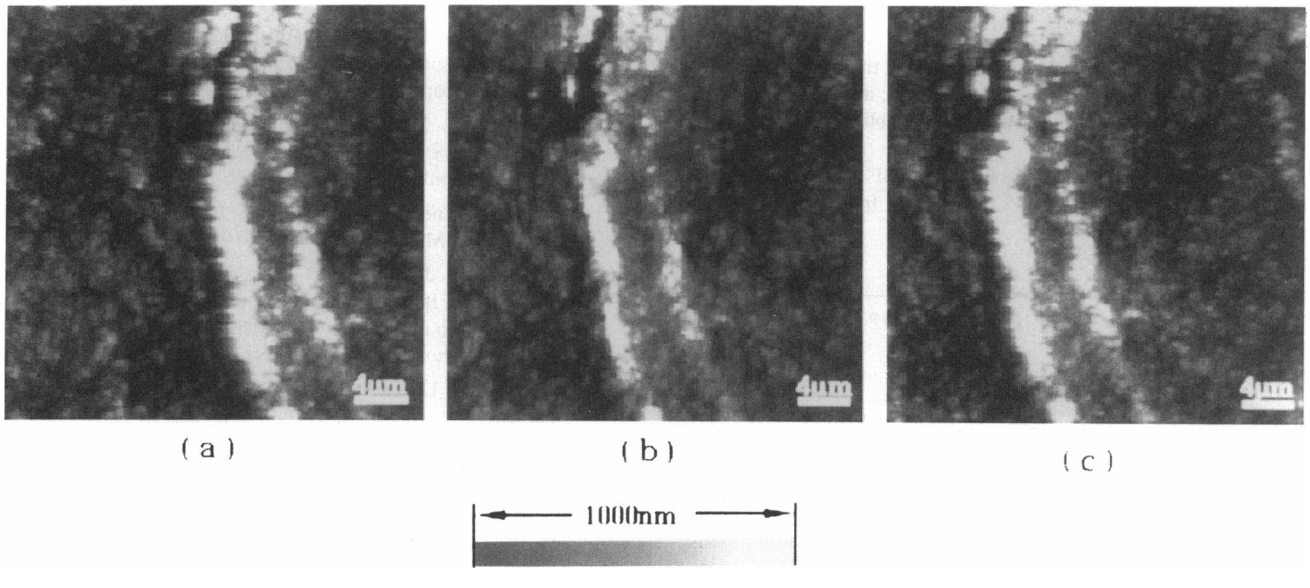

FIGURE 4 Intermediate magnification AFM images (49,000 × 49,000 nm) of the concentric structure of osteonal lamellae under 2.5 nN (*a*), 209 nN (*b*), and 2.6 nN (*c*). The height of the bright stripes at the center decreased under 209 nN.

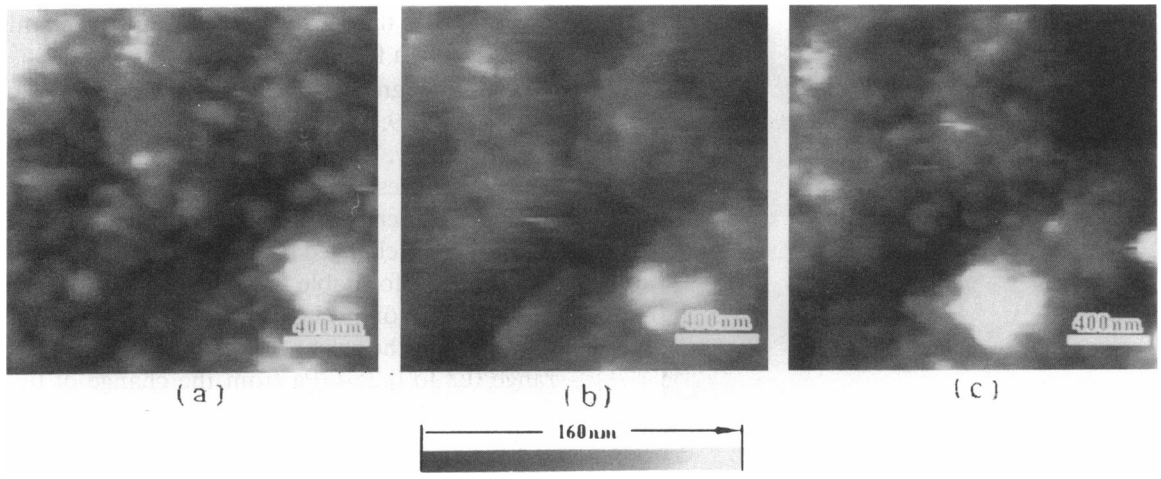

FIGURE 5 High magnification images of an osteonal lamellum under 2.5 nN (*a*), 205 nN (*b*), and 2.5 nN (*c*). The "blobs" vary in size from 50 to 500 nm. The image blurs under 205 nN and the original contrast is not recovered when the force is reduced (*c*).

We obtain 1.2 to 1.5 GPa, which is rather larger than any of the microscopic measurements (except on the inter-"blob" region described above). The discrepancy is too large to be accounted for by the possible range of values for Poisson's constant. The AFM data are sensitive to surface properties and it is quite possible that our sample preparation caused demineralization of the surface region. The solubility of apatite is orientation dependent and there can be different amounts of noncollagenous organic matter distributed over the crystallite faces, thereby affecting solubility. With further development of the AFM technique and experimentation with surface treatment, much can be done to elucidate the details of the mineralization at the exposed surface of the bone.

In summary, we have demonstrated that quantitative data on the elastic properties of a biological composite can be obtained with unprecedented resolution.

We are grateful to Elizabeth Page for preparing the sample, to Patrick Oden for useful comments on the manuscript, and to Paul Hansma who showed us a copy of reference 8 before publication.

This work was supported by grants from the NSF (DIR 89-20053) and ONR (N00014-90-J-1455) to S. Lindsay, and from the NIH (AGO 2325) to S. Lees.

Received for publication 17 February 1992 and in final form 12 May 1992.

REFERENCES

1. Binnig, G., C. F. Quate, and Ch. Gerber. 1986. Atomic force microscope. *Phys. Rev. Lett.* 56:930–933.
2. Drake, B., C. B. Prater, A. L. Weisenhorn, S. A. C. Gould, T. R. Albrecht, and C. F. Quate. 1989. Imaging crystals, polymers, and processes in water with the AFM. *Science (Wash. DC).* 243:1586–1589.
3. Weisenhorn, A. L., P. K. Hansma, T. R. Albrecht, and C. F. Quate. 1989. Forces in atomic force microscopy in air and water. *Appl. Phys. Lett.* 54:2651–2653.
4. Burnham, N. A., D. D. Dominguez, R. L. Mowery, and R. J. Colton. 1990. Probing the surface forces of monolayer films with an atomic force microscope. *Phys. Rev. Lett.* 64:1931–1934.
5. Mate, C. M., G. M. McClelland, R. Erlandsson, and S. Chiang. 1987. Atomic scale friction of a tungsten tip on a graphite surface. *Phys. Rev. Lett.* 59:1942–1945.
6. Erlandsson, E., G. Hadziioannou, C. M. Mate, G. M. McClelland, and S. Chiang. 1988. Atomic scale friction between the muscovite mica cleavage plane and a tungsten tip. *J. Chem. Phys.* 89:5190–5193.
7. Martin, Y., C. C. Williams, and H. K. Wickramasinghe. 1988. Tip-techniques for microcharacterization of materials. *Scanning Microsc.* 2:3–8.
8. Stern, J. E., B. D. Terris, H. J. Mamin, and D. Rugar. 1988. Deposition and imaging of local charge on insualtor surfaces using a force microscope. *Appl. Phys. Lett.* 53:2717–2719.
9. Burnham, N. A., and R. J. Colton. 1989. Measuring the nanomechanical properties and surface forces of materials using an atomic force microscope. *J. Vac. Sci. Technol.* A7:2906–2913.
10. Pethica, J. B. and W. C. Oliver. 1987. Tip-surface interactions in STM and AFM. *Physica Scripta.* T19:61–66.
11. Maivald, P., H. J. Butt, S. A. C. Gould, C. B. Prater, B. Drake, J. A. Gurley, V. B. Eilings, and P. K. Hansma. 1991. Using force-modulation to image surface elasticities in the atomic force microscope. *Nanotechnology.* In press.
12. Lees, S. 1982. Ultrasonic measurements of deer antler, bovine tibea and tympanic bulla. *J. Biomechanics.* 15:867–874.
13. Lees, S., J. M. Ahern, and M. Leonard. 1983. Parameters influencing the sonic velocity in compact calcified tissues of various species. *J. Acost. Soc. Amr.* 74:28–33.
14. Harley, R., D. James, A. Miller, and J. W. White. 1977. Phonons and the elastic moduli of collagen and muscle. *Nature (Lond.).* 267:285–287.
15. Randall, J., and J. M. Vaughan. 1979. Brillouin scattering in sys-

tems of biological significance. *Phil. Trans. R: Soc. Lond.* A293:341–348.

16. Cusack, S., and A. Miller. 1979. Determination of the elastic constants of collagen by Brillouin light scattering. *J. Mol. Biol.* 135:39–51.
17. Lees, S., N. J. Tao, and S. M. Lindsay. 1990. Studies of compact hard tissues and collagen by means of Brillouin light scattering. *Conn. Tissues Res.* 24:187–205.
18. Bonfield, W., and C. H. Li. 1966. Deformation and fracture of bone. *J. Appl. Phys.* 37:869–875, and see the book cited in reference 14.
19. Hancox, N. M. 1972. Biological Structure and Function 1, Biology of Bone. R. J. Harrison and R. M. H. McMinn, series editors. Cambridge University Press, New York. 199 pp.
20. Sneddon, I. N. 1965. The relation between load and penetration in the axisymmetric Boussinesq problem for a punch of arbirtatry profile. *Int. J. Eng. Sci.* 3:47–56.
21. Martin, B. R., and D. B. Burr. 1989. Structure, function and adaptation of compact bone. Raven Press, New York. p. 31.
22. Reilly, D. T., and A. H. Burstein. The elastic and ultimate properties of compact bone tissue. *J. Biomech.* 8:393–405.